Available online at www.sciencedirect.com
SCIENCE DIRECT
International Journal of Mass Spectrometry 249–250 (2006) 112–119
International Journal of Mass Spectrometry
www.elsevier.com/locate/ijms

Stereoselective noncovalent interactions of monosaccharides with hydrazine

Gianluca Giorgi [a], Maurizio Speranza [b,*]

[a] *Dipartimento di Chimica, Università di Siena, Via Aldo Moro, I-53100 Siena, Italy*
[b] *Dipartimento di Studi di Chimica e Tecnologia delle Sostanze Biologicamente Attive, Università di Roma "La Sapienza", P.le Aldo Moro 5, I-00185 Roma, Italy*

Received 31 October 2005; received in revised form 22 December 2005; accepted 27 December 2005
Available online 13 February 2006

In memory of Professor Chava Lifshiz in recognition of her outstanding contributions for many decades to gas-phase ion chemistry and physics.

Abstract

Proton-bound complexes between underivatized monosaccharides and hydrazine have been generated in an ion trap mass spectrometer by electrospray ionization (ESI) and their collision induced decomposition (CID) investigated. The CID spectra of the selected complexes are invariably characterized by losses of hydrazine and several water molecules in proportions and at collision energies which markedly depend upon the nature and the structural features of the specific monosaccharide. Structural analysis of the proton-bound monosaccharide/hydrazine complexes at the B3LYP/6-31G(d,p) level of theory allowed to interpret the mass spectrometric results in terms of the specific intracomplex interactions between the amine and the various functional groups of the monosaccharide.

Keywords: Glucosides; Hydrazine; Structural discrimination; Noncovalent complexes; Mass spectrometry

1. Introduction

Biomolecules mainly "communicate" with the surroundings through noncovalent interactions. Electrostatic forces, hydrogen bonds, hydrophobic and van der Waals interactions allow the formation of complexes like enzyme–substrate, protein–ligand, protein–protein, antigen–antibody, carbohydrate–protein adducts [1,2]. Albeit such interactions are much weaker (10–100 times) than covalent bonds, nevertheless they are of great importance. Large amplitude motion for noncovalent complex modes can play a crucial role in the dynamical processes connecting different minima on the free energy surface of a biological process. This means that a noncovalent aggregate should be thought as a dynamic system which cannot be described in terms of a well-defined fixed structure.

Carbohydrates are ubiquitous chiral compounds implicated in a host of biological functions. Either alone or as constituents of glycoproteins, proteoglycans and glycolipids, carbohydrates are mediators of a number of cellular events, such as intra- and extracellular recognition, differentiation, proliferation, signal transduction, and in numerous (patho)physiological processes [3–5]. As biological function and morphology are strongly correlated, the variety of structural and stereochemical features of carbohydrates are expected to mirror the complexity of noncovalent interactions they can establish in biological aggregates.

Such a complicate landscape represents a challenge for mass spectrometry (MS). Although MS is traditionally regarded as a "blind" tool for stereochemical determination, a body of evidence is nowadays available witnessing the potential of such a technique for structural analysis [6–8]. Soft ionization methods, such as electrospray (ESI) and matrix-assisted laser desorption (MALDI), in conjunction with tandem mass spectrometry (MS/MS) have been mainly used. Recently, Von Seggern and Cotter have studied noncovalent complexes of biologically interesting oligosaccharides by atmospheric pressure MALDI [9].

* Corresponding author. Tel.: +39 06 49913497; fax: +39 06 49913602.
E-mail address: maurizio.speranza@uniroma1.it (M. Speranza).

1387-3806/$ – see front matter © 2006 Elsevier B.V. All rights reserved.
doi:10.1016/j.ijms.2005.12.050

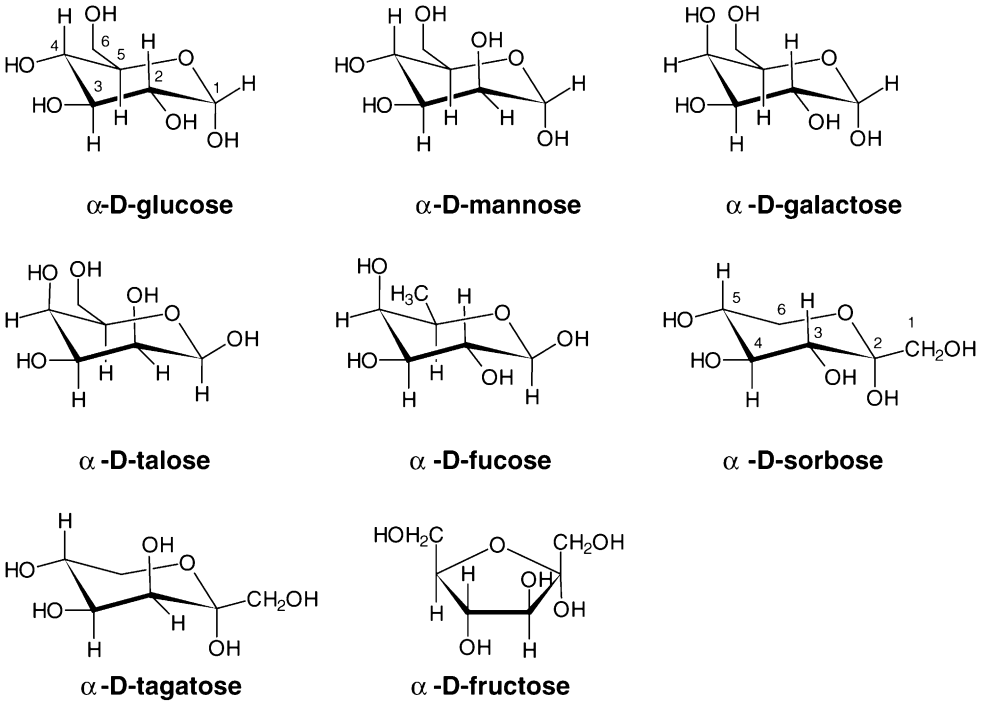

Scheme 1.

They have shown that the structure of the saccharides influences the number and strength of intermolecular hydrogen bonds. A number of noncovalent complexes [10–12], including those between carbohydrates and proteins [13], have been characterized by ESI-MS/MS. Wang, Kitova and Klassen used ESI in conjunction with a Fourier-transform ion cyclotron resonance analyzer (ESI-FT-ICR), to measure the affinity of a carbohydrate toward a protein [14]. They showed that a good correlation exists between solution [15] and gas-phase affinity data. The geometrical isomers of aliphatic and cyclic diols have been differentiated by Tabet and coworkers through formation of $FeCl^+$-bound adducts with an enantiomerically pure saccharide [16]. The kinetic method developed by Cooks has been also applied in the quantitative analysis of chiral species [17–19]. Enantiodifferentiation of glucose, mannose, galactose and ribose was obtained by collision induced dissociation (CID) of their noncovalent complexes containing a reference modified amino acid and a bivalent transition metal ion [20].

The present study is aimed at providing more insights into the correlation between the structure and the stereochemistry of underivatized monosaccharides (S) and their interactions in proton-bound complexes with suitable acceptors. The α-D-fructose (**fru**) was selected, together with the following α-D-glucopyranoses: glucose (**glu**), mannose (**man**), galactose (**gal**), talose (**tal**), tagatose (**tag**), sorbose (**sor**), and fucose (**fuc**) (Scheme 1). After a long search of the most appropriate acceptor, the choice fell on N_2H_4 for two reasons: (i) its proton affinity (PA = 203.9 kcal mol^{-1}) [21] is comparable to those estimated for underivatized monosaccharides [22]; and (ii) it reveals suitable for their structural discrimination (vide infra). The approach used is based on the CID of the corresponding $[S{\bullet}H{\bullet}N_2H_4]^+$ adducts in conjunction with theoretical calculations.

2. Experimental

The electrospray experiments were performed using a commercial LCQ-Deca ThermoFinnigan ion trap mass spectrometer, equipped with an ESI source and a syringe pump. Operating conditions for the ESI source were as follows: spray voltage, 4.5 kV; capillary temperature in the 150–190 °C range; sheath gas (He) flow rate, ca. 0.75 L/min). The experiments were conducted in the positive ion mode. Reported spectra represent the average of about 150 scans, each requiring 0.1 s. The selected gas phase complexes were generated by electrospraying water/methanol solutions containing equimolar amounts of the hydrazine and the monosaccharide, 1.5 mM each. The sample was infused via a syringe pump at a flow rate of 5 μl/min. In the full scan MS/MS mode, the ion of interest was firstly isolated by broadband ejection of the accompanying ions and then subjected to collision induced dissociation (CID; colliding gas: He; collision energy: 0.5–1.0 eV (laboratory frame)).

The geometrical structures of the proton-bound monosaccharide/hydrazine clusters have been optimized with a density functional theory (DFT) approach using a medium size basis set by using the Gaussian 03 package [23]. The DFT Hamiltonian is Becke's three-parameter hybrid functional with the Lee, Yang, and Parr correlation functional [24]; the basis set is the 6–31 G(d,p). The final lowest-energy geometries were confirmed as a minimum on the molecular potential energy surface by normal-mode vibrational frequency calculations that produced all real frequences. Zero-point vibrational energies and statistical thermodynamic properties at 298.15 K and 1 atm were calculated at the B3LYP 6-31G(d,p) level of theory. All calculations were performed using a IBM SP5 supercomputer at Cineca (Bologna, Italy).

3. Results

The ESI-MS spectra of S/N_2H_4 hydroalcoholic mixtures are characterized by the presence of abundant signals corresponding to the $[S{\bullet}H{\bullet}N_2H_4]^+$ adducts. These noncovalent complexes are very persistent under the experimental conditions adopted, whereas they undergo distinctive and specific decompositions when colliding with He inside the ion trap. Fig. 1a–d illustrate the 0.7 eV (laboratory frame) collision MS/MS spectra of the noncovalent $[S{\bullet}H{\bullet}N_2H_4]^+$ (S = **glu**, **man**, **gal**, and **tal**) complexes. Those of the noncovalent $[S{\bullet}H{\bullet}N_2H_4]^+$ (S = **fru**, **tag**, **sor**, and **fuc**) complexes, taken under the same conditions, are shown in Fig. 2a–d, respectively. The energy-resolved MS/MS diagrams of $[S{\bullet}H{\bullet}N_2H_4]^+$ (S = **glu**, **man**, **gal**, and **tal**) (E_{coll} = 0.5–1.0 eV, lab frame) are reported in Fig. 3. Those of $[S{\bullet}H{\bullet}N_2H_4]^+$ (S = **fru**, **tag**, and **sor**) are given in Fig. 6S of the Supplementary Information.

All the $[S{\bullet}H{\bullet}N_2H_4]^+$ complexes, except that with S = **fuc** (*m*/*z* 197), have the same *m*/*z* value (*m*/*z* 213). Their low-energy CID spectra are invariably characterized by the loss of hydrazine and several water molecules (Figs. 1 and 2). However, the mode of release of these molecules is found to depend upon the nature and the structural features of the S component. Thus, while the complex with **tal** (Fig. 1d) eliminates predominantly neutral N_2H_4 at all collision energies (Fig. 3d), that with **glu** (Fig. 1a) mainly eliminates one or two H_2O molecules at low collision energies, the loss of N_2H_4 being appreciable only at $E_{coll} \geq 0.7$ eV (Fig. 3a). The elimination of N_2H_4 is prevented in the complex with **gal** as well (Figs. 1c and 3c). Indeed, in this systems. N_2H_4 is released only from the relevant $[(S{\bullet}H{\bullet}N_2H_4){-}H_2O]^+$ fragment in competition with the loss of a further H_2O molecule. Finally, the complex with **man** (Figs. 1b and 3b) is able to release indiscriminately N_2H_4 and one or two H_2O molecules. A distinctive feature of the CID spectra of the $[S{\bullet}H{\bullet}N_2H_4]^+$ (S = **fru**, **sor**, and **fuc**) complexes is the exclusive loss of a single water molecule (Fig. 2a, c and d). No appreciable departure of either N_2H_4 or a second H_2O molecule is observed. In contrast, low-energy CID spectrum of the complex with **tag** (Fig. 2b) somewhat resembles that of the complex with **glu** (Fig. 1a), characterized by the exclusive release of a H_2O molecule. In both complexes, the loss of N_2H_4 is detected only at $E_{coll} \geq 0.7$ eV (Fig. 3a and Supplementary Information).

The B3LYP/6-31G(d,p)-calculated minimum-energy structures of the $[S{\bullet}H{\bullet}N_2H_4]^+$ (S = **glu**, **man**, **gal**, **tal**, and **tag**) potential energy surfaces are illustrated in Fig. 4a–e, respectively. The corresponding total energy corrected for the zero-point vibrational energies (ZPVE) are given in Table 1S of Supplementary Information. In the most stable $[S{\bullet}H{\bullet}N_2H_4]^+$ (S = **glu**) structure, the N_2H_4 molecule is proton-bound to both the $^{(3)}$OH (bond length: 1.73 Å) and $^{(4)}$OH (bond length: 1.73 Å) groups of **glu** (Scheme 1 and Fig. 4a). These interactions are accompanied by the intramolecular $^{(4)}$O–H•••$^{(5)}$O bonding (bond length: 1.78 Å). The presence of the axial hydroxyl group at the $^{(2)}$C of **man** allows the corresponding most stable $[S{\bullet}H{\bullet}N_2H_4]^+$ complex to acquire a structure wherein the N_2H_4 molecule is proton-bound to both the $CH_2{}^{(5)}$OH group (bond length: 1.73 Å)

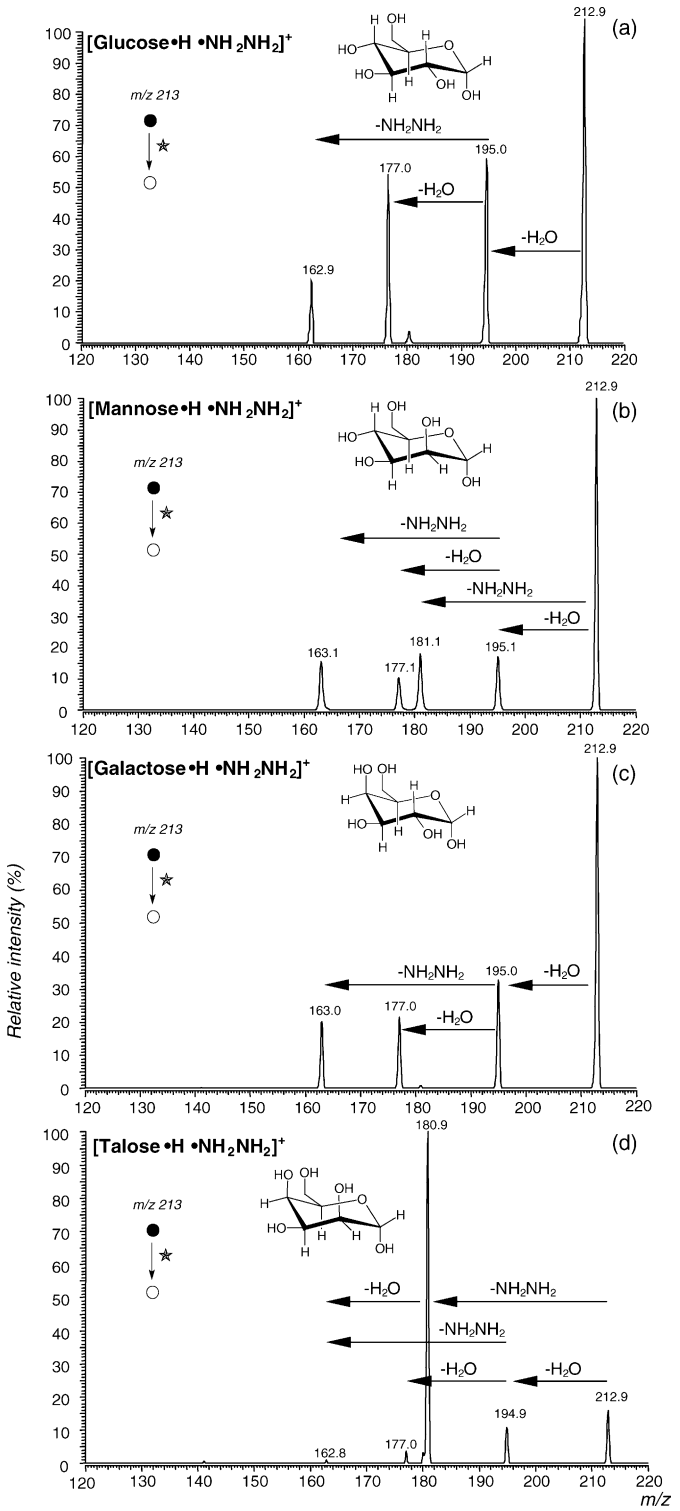

Fig. 1. Low-energy collision MS/MS spectra of noncovalent complexes of $[S{\bullet}H{\bullet}N_2H_4]^+$ (S = **glu** (a), **man** (b), **gal** (c), and **tal** (d); E_{coll} = 0.7 eV (lab frame)).

and $^{(2)}$OH center (bond length: 1.74 Å) (Fig. 4b). Similar multiple interactions are prevented in $[S{\bullet}H{\bullet}N_2H_4]^+$ (S = **glu**) by the opposite configuration of the $^{(2)}$C center. In contrast, the very similar total energies of $[S{\bullet}H{\bullet}N_2H_4]^+$ (S = **glu** and **man**) (see Table 1S in Supplementary Information) suggest the possibility

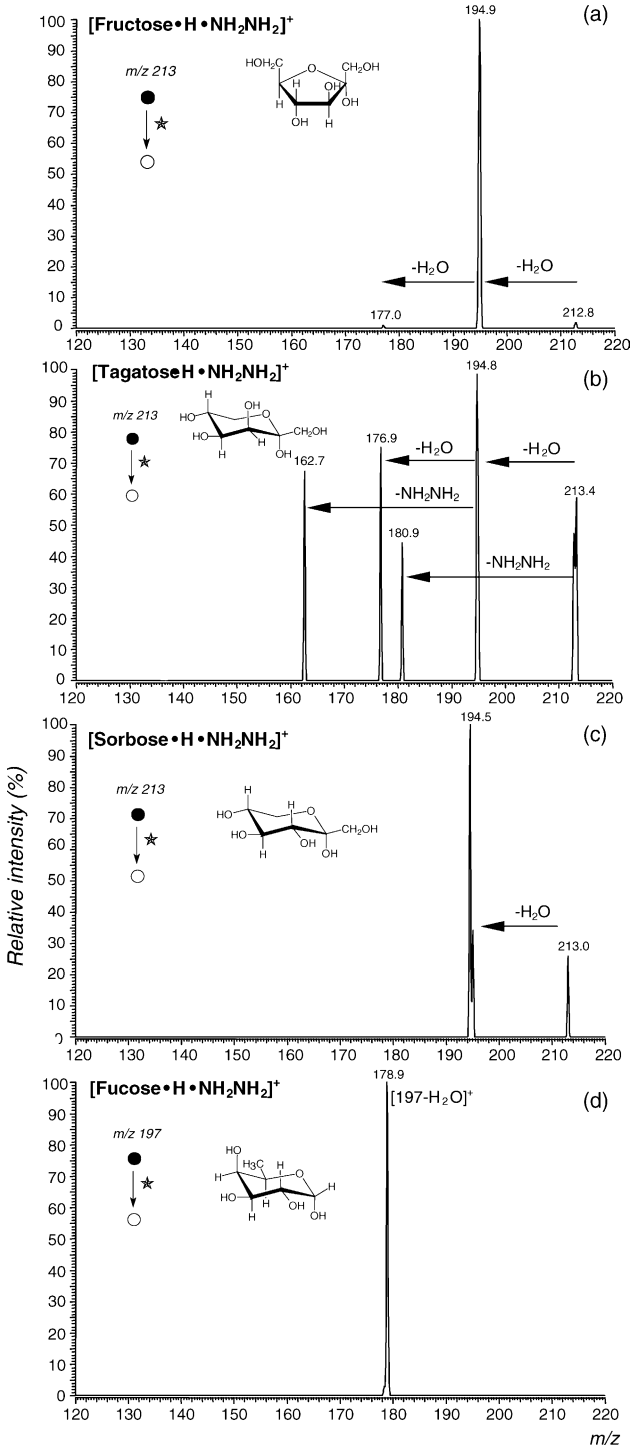

Fig. 2. Low-energy collision MS/MS spectra of noncovalent complexes of $[S{\bullet}H{\bullet}N_2H_4]^+$ (S = **fru** (a), **tag** (b), **sor** (c), and **fuc** (d); E_{coll} = 0.7 eV (lab frame)).

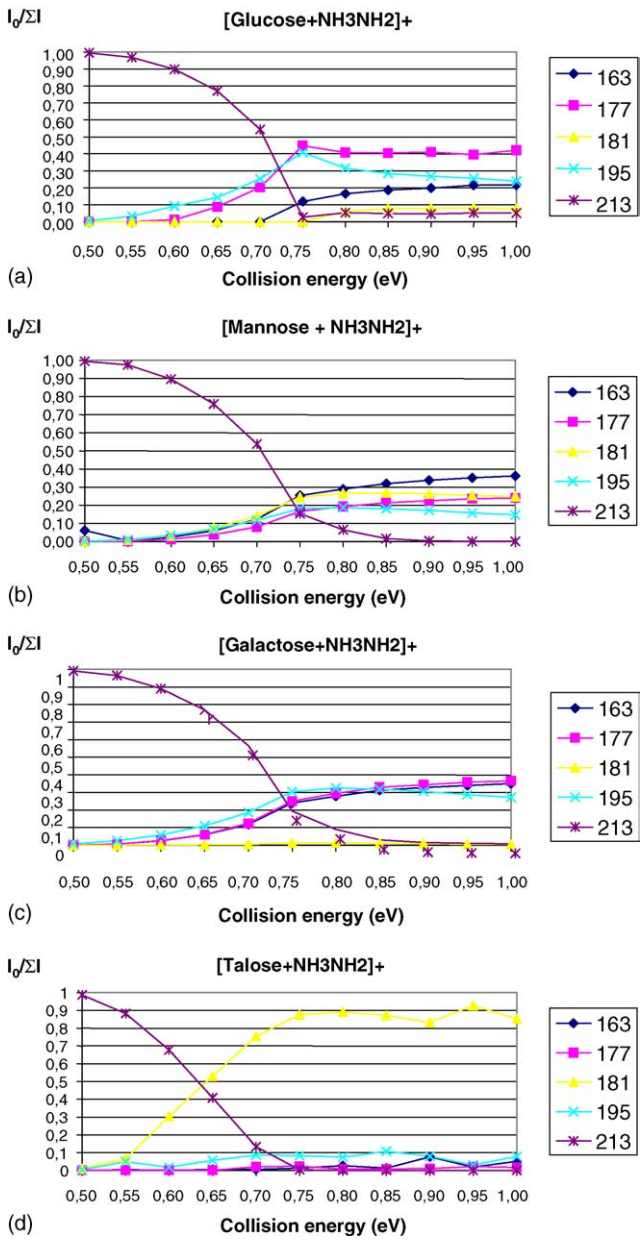

Fig. 3. Energy-resolved MS/MS diagrams of $[S{\bullet}H{\bullet}N_2H_4]^+$ (S = **glu** (a), **man** (b), **gal** (c), and **tal** (d); E_{coll} = 500–1000 meV (lab frame)).

that N_2H_4 may interact with the $^{(3)}$OH and $^{(4)}$OH of man as well, much like in the $[S{\bullet}H{\bullet}N_2H_4]^+$ (S = **glu**) complex. Indeed, the second most stable $[S{\bullet}H{\bullet}N_2H_4]^+$ (S = **man**) structure exhibits the N_2H_4 molecule proton-bound to both the $^{(3)}$OH (bond length: 1.72 Å) and $^{(4)}$OH (bond length: 1.70 Å) of **man** (see Supplementary Information). The presence of the axial hydroxyl group at $^{(4)}$C and of the equatorial hydroxyl group at $^{(2)}$C of $[S{\bullet}H{\bullet}N_2H_4]^+$ (S = **gal**) hinders the establishment of the intense proton-bonds present in the $[S{\bullet}H{\bullet}N_2H_4]^+$ (S = **glu** and **man**) complexes. In this case, the N_2H_4 molecule is best coordinated by the $^{(1)}$OH (bond length: 1.77 Å) and $CH_2{}^{(5)}$OH (bond length: 1.80 Å) of **gal** (Fig. 4c). The $[S{\bullet}H{\bullet}N_2H_4]^+$ (S = **tal**) exhibits the same kind of intermolecular interactions of $[S{\bullet}H{\bullet}N_2H_4]^+$ (S = **man**). Both structures are characterized by two proton-bonds between N_2H_4 and the $CH_2{}^{(5)}$OH and $^{(2)}$OH groups of the monosaccharide (Fig. 4d). The only difference arises from the presence of the additional H-bond between hydrazine and the axial $^{(4)}$OH group of the monosaccharide in $[S{\bullet}H{\bullet}N_2H_4]^+$ (S = **tal**) which is absent in $[S{\bullet}H{\bullet}N_2H_4]^+$ (S = **man**). This additional interaction is established to the expenses of the specific proton-bond with the $^{(2)}$OH center (cfr. N–H•••$^{(2)}$O

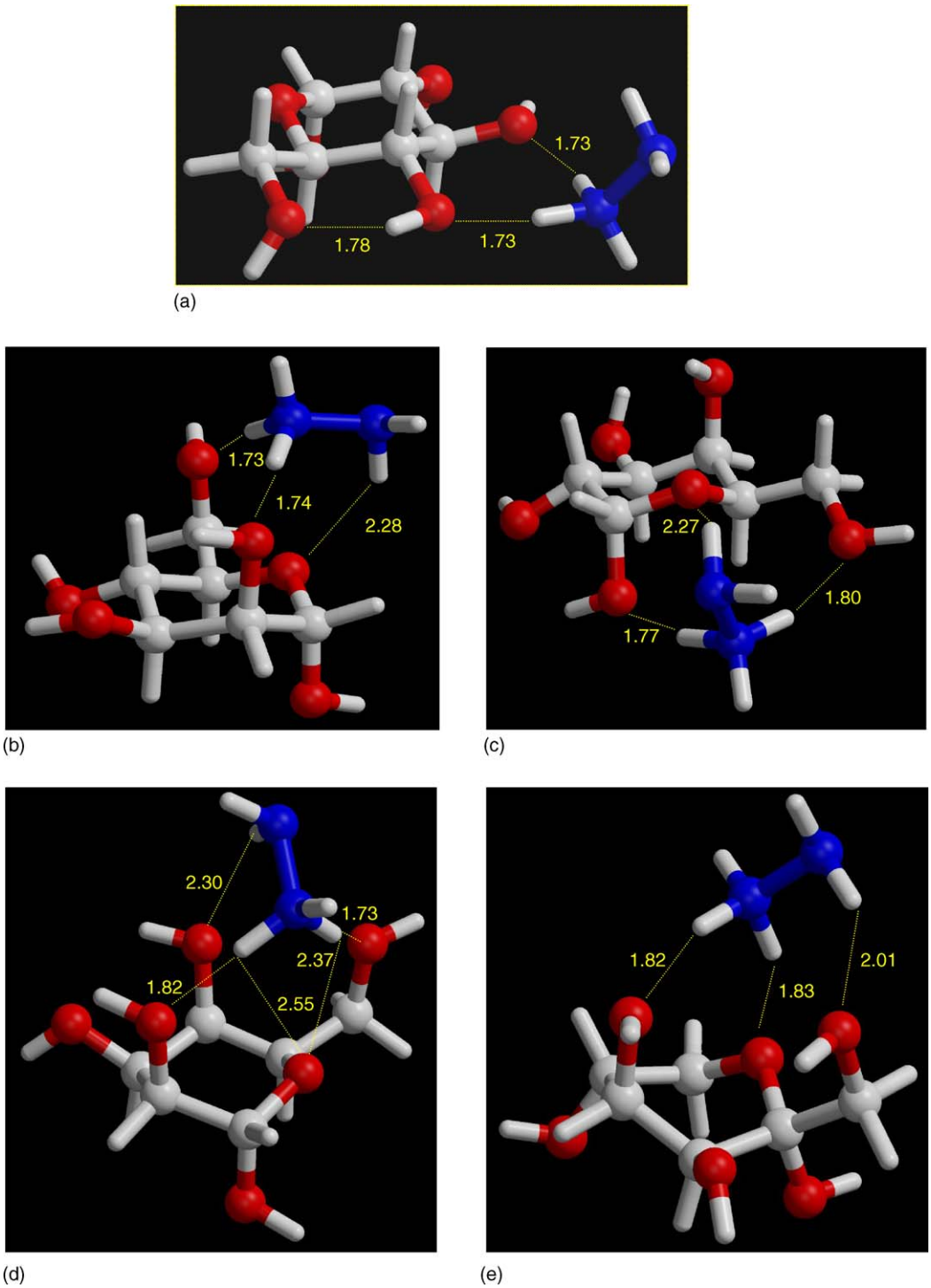

Fig. 4. Lowest-energy B3LYP/6-31G(d,p)-optimized structures of $[S{\bullet}H{\bullet}N_2H_4]^+$ (S = **glu** (a), **man** (b), **gal** (c), **tal** (d), and **tag** (e)).

bond length: 1.82 Å (S = **tal**), 1.74 Å (S = **man**)). Finally, the $[S{\bullet}H{\bullet}N_2H_4]^+$ (S = **tag**) structure presents a distinctive feature, relative to the other structures of Fig. 4. Indeed, it is the only one with the pyranose ring in the boat conformation. This is due to the fact that the N_2H_4 molecule establishes energy favoured multiple proton-bonds with both the $^{(6)}$O (bond length: 1.83 Å), and the axial $^{(4)}$OH (bond length: 1.82 Å) (Scheme 1 and Fig. 4e). These interactions are accompanied by H-bonding between the $^{(2)}$NH group of hydrazine and the $CH_2{}^{(1)}$OH groups of **tag** (bond length: 2.01 Å).

4. Discussion

The observation of significant amounts of the $[(S{\bullet}H{\bullet}N_2H_4)-nH_2O]^+$ (n = 1,2) and $[(S{\bullet}H)-mH_2O]^+$ (m = 0,1) fragments from the CID of the $[S{\bullet}H{\bullet}N_2H_4]^+$ complexes indicates that

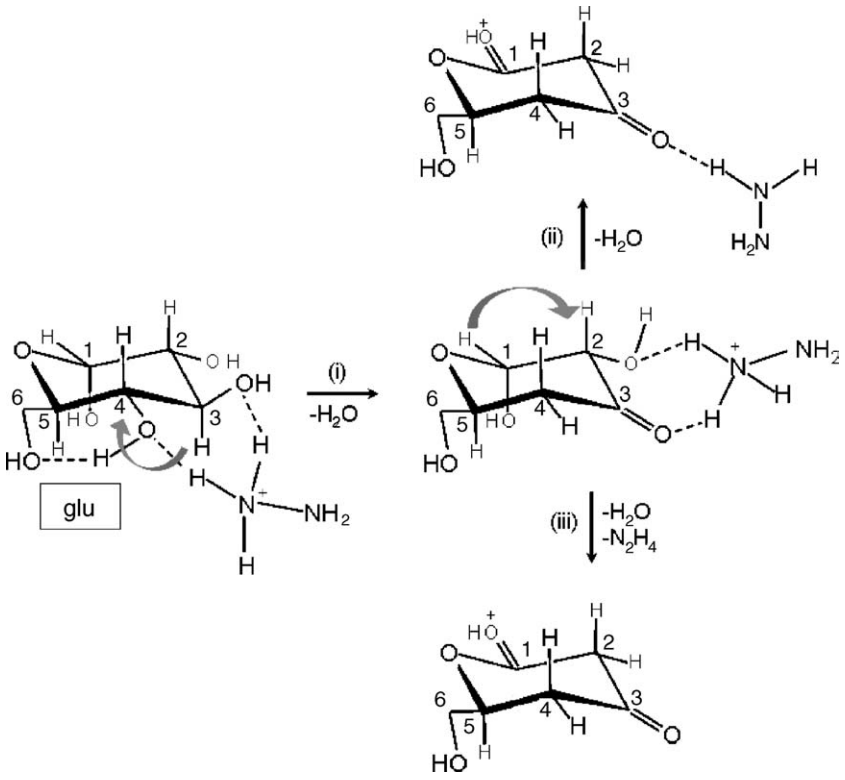

Scheme 2.

the gas-phase basicity (GB) of the S component as well as of its dehydrated form is comparable with that of hydrazine (GB = 196.6 kcal mol^{-1}) [21,22]. Although no attempt was made to ascertain the origin of the eliminated H_2O, these considerations allow us to advance some hypotheses about possible structures for the dehydrated $[(S\bullet H)–mH_2O]^+$ (m = 0,1) fragments.

Among the $[S\bullet H\bullet N_2H_4]^+$ structures of Fig. 4, that with S = **glu** is the only one wherein the $CH_2{}^{(5)}OH$ group does not act as proton-bond acceptor from hydrazine (Fig. 4a). This means that the $CH_2{}^{(5)}OH$ group of **glu** is able to act as proton acceptor from the adjacent $H^{(4)}O\bullet\bullet\bullet H^+\bullet\bullet\bullet N_2H_4$ system and, therefore, to catalyze the loss of the H_2O molecule from the $^{(4)}C$ of the saccharide. The release of the H_2O molecule may be assisted by 1,2-hydrogen shift with formation of the corresponding ketone coordinated to the hydrazine molecule through the $C{=}^{(3)}O\bullet\bullet\bullet H^+\bullet\bullet\bullet N_2H_4$ bonding (path (i) of Scheme 2). This hypothesis is consistent with the pronounced basicity of substituted cyclohexanones [21] and is corroborated by the following consideration. The loss of a further water molecule from the $[(S\bullet H\bullet N_2H_4)–H_2O]^+$ fragment requires the establishment of a relatively strong proton-bond between N_2H_4 and the residual OH group of the $[(S\bullet H)–H_2O]^+$ moiety which will be involved in the dehydration. This condition can be reached by allowing the N_2H_4 molecule to establish multiple interactions with both the $C{=}^{(3)}OH^+$ and the vicinal $^{(2)}OH$ group of $[(S\bullet H)–H_2O]^+$. This cooperative proton-bond arrangement is suitable for promoting the release of a further water molecule by a mechanism similar to that of the first water loss (paths (ii) and (iii) of Scheme 2 and Fig. 3a).

The predominant elimination of a water molecule from the low-energy CID of $[S\bullet H\bullet N_2H_4]^+$ (S = **gal**) can be accounted for by the $H^{(1)}O\bullet\bullet\bullet H^+\bullet\bullet\bullet N_2H_4$ interaction which favours the loss of the relevant H_2O molecule, anchimerically assisted by the adjacent C-H bond in the antiperiplanar position (Figs. 3c and 4c) [25,26]. In the resulting $[(S\bullet H\bullet N_2H_4)–H_2O]^+$ fragment, the hydrazine moiety is weakly interacting with the $CH_2{}^{(5)}OH$ group of **gal** and, thus, it is located far away from the formed $C{=}^{(2)}OH^+$ group. The consequence is that further water elimination is not as easy as in the case of $[(S\bullet H\bullet N_2H_4)–H_2O]^+$ (S = **glu**) and, therefore, release of N_2H_4 efficiently competes with the second water loss (Fig. 3c).

The assistance of the $CH_2{}^{(5)}OH$ group of **gal** and **glu** in the multiple dehydration of the corresponding $[S\bullet H\bullet N_2H_4]^+$ complexes is outlined by the absence of the same process in the CID of the complex with **fuc**, where the same position is occupied by a CH_3 group (Fig. 2d). It is plausible that, in $[(S\bullet H\bullet N_2H_4)–H_2O]^+$ (S = **fuc**), further fragmentations are hindered by the large energy required for the unassisted departure of the first H_2O molecule.

The prompt elimination of a water molecule from the low-energy CID of $[S\bullet H\bullet N_2H_4]^+$ (S = **tag**) is attributed to the $H^{(4)}O\bullet\bullet\bullet H^+\bullet\bullet\bullet N_2H_4$ interaction which promotes the loss of the H_2O molecule from the $^{(4)}C$ center, assisted by the adjacent antiperiplanar $^{(3)}C–H$ bond (Figs. 2b and 4e). A similar process takes place in $[S\bullet H\bullet N_2H_4]^+$ (S = **man**). Here, it is the $H^{(2)}O\bullet\bullet\bullet H^+\bullet\bullet\bullet N_2H_4$ interaction which induces the elimination of the H_2O molecule, possibly assisted by the adjacent $^{(3)}C–H$ bond (Figs. 3b and 4b). This process is accompanied by the release of N_2H_4, whereas the elimination of the same molecule from $[S\bullet H\bullet N_2H_4]^+$ (S = **tag**) is observed only

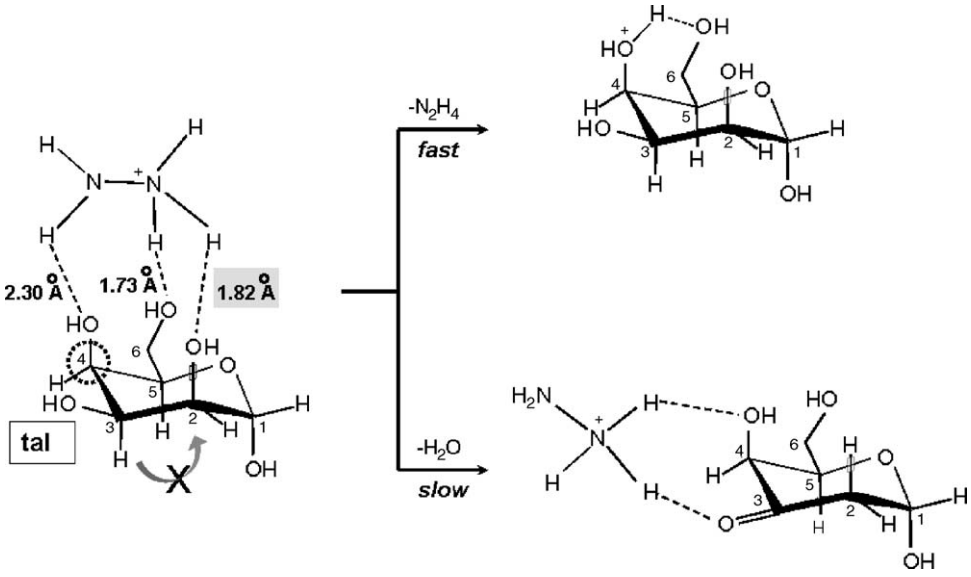

Scheme 3.

at collision energies above 0.65 eV (Fig. 3b and Supplementary Information). A possible explanation for such a difference may be found in the observation that, in the $[(S{\bullet}H{\bullet}N_2H_4)–H_2O]^+$ (S = **man**) fragment, the N_2H_4 molecule can hardly interact simultaneously with the $CH_2{}^{(5)}OH$ and $^{(6)}O$ centers and the incipient $C{=}^{(3)}OH^+$ one. In the $[(S{\bullet}H)–H_2O]^+$ (S = **tag**) fragment, instead, the $C{=}^{(3)}OH^+$, $CH_2{}^{(1)}OH$, and $^{(6)}O$ centers are adjacent each others and, therefore, suitable for multiple interactions with the N_2H_4 molecule.

As pointed out before, the proton bond between N_2H_4 molecule and the $^{(2)}OH$ center of S in $[S{\bullet}H{\bullet}N_2H_4]^+$ (S = **tal**) (bond length: 1.82 Å; Fig. 4d) is appreciably weaker than the same interaction in $[S{\bullet}H{\bullet}N_2H_4]^+$ (S = **man**) (bond length: 1.74 Å; Fig. 4b). This is due to the opposite configuration of the $^{(4)}C$ center in the corresponding saccharides (Schemes 3 and 4). This situation somewhat reduces the efficiency of the elimination of the H_2O molecule from the $^{(2)}C$ site of $[S{\bullet}H{\bullet}N_2H_4]^+$ (S = **tal**; Scheme 3), if compared to that of the same process in $[S{\bullet}H{\bullet}N_2H_4]^+$ (S = **man**; Scheme 4). The result is that the CID of $[S{\bullet}H{\bullet}N_2H_4]^+$ (S = **tal**) proceeds almost exclusively via the elimination of N_2H_4 (Figs. 1d and 3d).

Accurate analysis of the energy resolved MS/MS spectra of the $[S{\bullet}H{\bullet}N_2H_4]^+$ (S = **glu**, **man**, **gal**, and **tal**) complexes (Fig. 3), reveals that their 50% survival yield ($SY_{1/2}$) corresponds to collision energies close to 700 meV, except for the complex with the S = **tal** epimer which shows a $SY_{1/2}$ value below 650

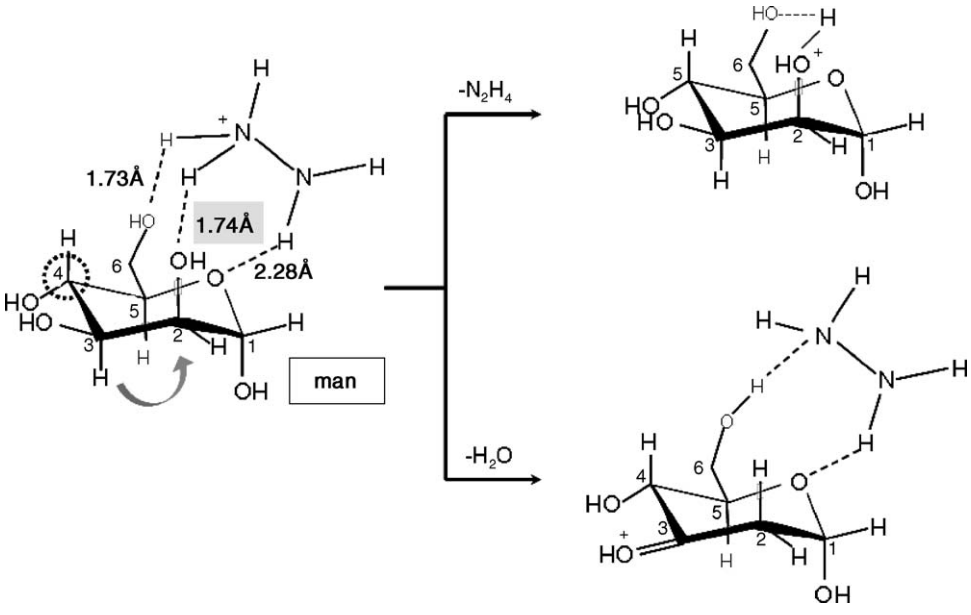

Scheme 4.

meV (Fig. 3b). The identical $SY_{1/2}$ energy for $[S{\bullet}H{\bullet}N_2H_4]^+$ (S = **glu**, **man**, and **gal**) is a symptom of their very similar structure, whereas the lower $SY_{1/2}$ energy for $[S{\bullet}H{\bullet}N_2H_4]^+$ (S = **tal**) is attributable to the comparatively weaker proton-bondings between the N_2H_4 and the **tal** moieties.

As pointed out before, CID of the $[S{\bullet}H{\bullet}N_2H_4]^+$ (S = **fuc**) promotes the exclusive loss of a single water molecule. The lack of further fragmentation of $[(S{\bullet}H{\bullet}N_2H_4)–H_2O]^+$ is attributed to the large energy required for the unassisted departure of the first H_2O molecule. The same reason may account for the exclusive loss of a single water molecule, observed with $[S{\bullet}H{\bullet}N_2H_4]^+$ (S = **sor**) as well (Fig. 2c). In this connection, it should be noted that the only important structural difference between $[S{\bullet}H{\bullet}N_2H_4]^+$ (S = **sor**) and $[S{\bullet}H{\bullet}N_2H_4]^+$ (S = **tag**) is the opposite configuration of their $^{(3)}C$ center. It is therefore plausible that the two complexes exhibit a similar most stable structure (Fig. 4e). In this view, the $H^{(4)}O{\bullet\bullet\bullet}H^+{\bullet\bullet\bullet}N_2H_4$ interaction in $[S{\bullet}H{\bullet}N_2H_4]^+$ (S = **sor**) induces the unassisted loss of the corresponding H_2O molecule, since no adjacent antiperiplanar C–H bonds are available. As for $[S{\bullet}H{\bullet}N_2H_4]^+$ (S = **fuc**), such an energy-demanding unassisted dehydration prevents further fragmentation of $[S{\bullet}H{\bullet}N_2H_4]^+$ (S = **sor**).

5. Conclusions

Structural discrimination of a series of underivatized monosaccharides has been achieved through the energy-resolved CID fragmentation patterns of their noncovalent complexes with hydrazine. Their CID spectra are invariably characterized by stereoselective losses of hydrazine and several water molecules in proportions and at collision energies which significantly depend upon the nature and the structural features of the specific monosaccharide. Structural analysis of the B3LYP/6-31G(d,p)-computed most stable monosaccharide/hydrazine complexes allowed to interpret the mass spectrometric results in terms of the specific intracomplex interactions between the amine and the functional groups of the monosaccharide. The resulting picture provides a novel viewpoint about the factors determining the interactions of monosaccharides with receptor sites and proteins and, therefore, their biological functions.

Acknowledgements

This work was supported by the Ministero dell'Istruzione, dell'Università, e della Ricerca (MIUR-COFIN) and by the Consiglio Nazionale delle Ricerche (CNR).

Appendix A. Supplementary data

Supplementary data associated with this article can be found, in the online version, at doi:10.1016/j.ijms.2005.12.050.

References

[1] J.A. Loo, Mass Spectrom. Rev. 16 (1997) 1.
[2] T.D. Veenstra, Biophys. Chem. 79 (1999) 63.
[3] A.L. Lehninger, D.L. Nelson, M.M. Cox, Principes de Biochimie, second ed., Flammarion, Paris, 1994.
[4] A. Helenius, M. Aebi, Science 291 (2001) 2364.
[5] L. Wells, K. Vosseller, G.W. Hart, Science 291 (2001) 2376.
[6] J.S. Splitter, F. Turecek, Applications of Mass Spectrometry to Stereochemistry, VCH Publishers, New York, 1993.
[7] A. Mandelbaum, The Encyclopedia of Mass Spectrometry, vol. 4, Elsevier, 2005, p. 410 (Chapter 3).
[8] T.H. Morton, The Encyclopedia of Mass Spectrometry, vol. 4, Elsevier, 2005, p. 433 (Chapter 3).
[9] C.E. Von Seggern, R.J. Cotter, J. Am. Soc. Mass Spectrom. 14 (2003) 1158.
[10] A. Ayed, A.N. Krutchinsky, W. Ens, K.G. Standing, H.W. Duckworth, Rapid Commun. Mass Spectrom. 12 (1998) 339.
[11] M.J. Greig, H. Gaus, L.L. Cummins, H. Sasmor, R.H. Griffey, J. Am. Chem. Soc. 117 (1995) 10765.
[12] T.J.D. Jorgensen, P. Roepstorff, A.J.R. Heck, Anal. Chem. 70 (1998) 4427.
[13] B. Ganem, Y.T. Li, J.D. Henion, J. Am. Chem. Soc. 113 (1991) 7818.
[14] W. Wang, E.N. Kitova, J.S. Klassen, Anal. Chem. 75 (2003) 4945.
[15] D.R. Bundle, Methods Enzymol. 247 (1994) 288.
[16] V. Carlesso, C. Afonso, F. Fournier, J.C. Tabet, C. R. Comptes Rendue Chimie 6 (2003) 623.
[17] T.K. Majumdar, F. Clairet, J.-C. Tabet, R.G. Cooks, J. Am. Chem. Soc. 114 (1992) 2897.
[18] W.Y. Shen, P.S.H. Wong, R.G. Cooks, Rapid Commun. Mass Spectrom. 11 (1997) 71.
[19] K. Vekey, G. Czira, Anal. Chem. 69 (1997) 1700.
[20] D.V. Augusti, F. Carazza, R. Augusti, W.A. Tao, R.G. Cooks, Anal. Chem. 74 (2002) 3458.
[21] http://webbook.nist.gov/chemistry/name-ser.html.
[22] No information is presently available on the GB of underivatized monosaccharides. Some of their structural analogues, such as *cis*-1,2-dihydroxycyclohexane, *cis*-1,2-dihydroxycyclopentane, 1,3-dihydroxypropane, and 1,2,3-trihydroxypropane have GB values ranging from ca. 196 to ca. 204 kcal mol−1 (ref. [21]).
[23] M.J. Frisch, G.W. Trucks, H.B. Schlegel, G.E. Scuseria, M.A. Robb, J.R. Cheeseman, J.A. Montgomery Jr., T. Vreven, K.N. Kudin, J.C. Burant, J.M. Millam, S.S. Iyengar, J. Tomasi, V. Barone, B. Mennucci, M. Cossi, G. Scalmani, N. Rega, G.A. Petersson, H. Nakatsuji, M. Hada, M. Ehara, K. Toyota, R. Fukuda, J. Hasegawa, M. Ishida, T. Nakajima, Y. Honda, O. Kitao, H. Nakai, M. Klene, X. Li, J.E. Knox, H.P. Hratchian, J.B. Cross, C. Adamo, J. Jaramillo, R. Gomperts, R.E. Stratmann, O. Yazyev, A.J. Austin, R. Cammi, C. Pomelli, J.W. Ochterski, P.Y. Ayala, K. Morokuma, G.A. Voth, P. Salvador, J.J. Dannenberg, V.G. Zakrzewski, S. Dapprich, A.D. Daniels, M.C. Strain, O. Farkas, D.K. Malick, A.D. Rabuck, K. Raghavachari, J.B. Foresman, J.V. Ortiz, Q. Cui, A.G. Baboul, S. Clifford, J. Cioslowski, B.B. Stefanov, G. Liu, A. Liashenko, P. Piskorz, I. Komaromi, R.L. Martin, D.J. Fox, T. Keith, M.A. Al-Laham, C.Y. Peng, A. Nanayakkara, M. Challacombe, P.M.W. Gill, B. Johnson, W. Chen, M.W. Wong, C. Gonzalez, J.A. Pople, Gaussian 03, Revision B.05, Gaussian, Inc., Pittsburgh, PA, 2003.
[24] A.D. Becke, J. Chem. Phys. 98 (1993) 5648.
[25] C. J: Collins, J.F. Eastham, in: S. Patai (Ed.), The Chemistry of Functional Groups, Wiley Interscience, New York, 1966 (Chapter 15).
[26] B. Rickborn, Comprehensive Organic Chemistry: The Pinacol Rearrangement, M. Trost (Ed.), vol. 3, 1991, p. 721 (Chapter 2).